OPEN

NPG Asia Materials (2017) 9, e445; doi:10.1038/am.2017.168
www.nature.com/am

ORIGINAL ARTICLE

Nature-inspired thermo-responsive multifunctional membrane adaptively hybridized with PNIPAm and PPy

Hyejeong Kim, Kiwoong Kim and Sang Joon Lee

Specialized plant tissues, such as the epidermis of a leaf covered with stomata, consist of soft materials with deformability and electrochemical properties to achieve specific functions in response to various environmental stimuli. Stimulus-responsive hydrogels with electrochemical properties are good candidates for imitating such special functionalities in nature and thus have great potential in a wide range of academic and industrial applications. However, hydrogel-incorporated conductive materials are usually mechanically rigid, which limits their application in other fields. In addition, the fabrication technology of structured functional hydrogels has low reproducibility due to the required multistep processing. Here, inspired by nature, specifically the stimulus-responsive functionalities of plants, a new thermo-responsive multifunctional hybrid membrane (HM) is synthesized through the *in situ* hybridization of conductive poly(pyrrole) (PPy) on a photopolymerized poly(*N*-isopropylacrylamide) (PNIPAm) matrix. The morphological and electrical properties of the fabricated HM are investigated to characterize various aspects of its multiple functions. In terms of morphology, the HM can be easily fabricated into various structures by smartly utilizing photopolymerization patterning, and it exhibits thermo-responsive deformability. In terms of functionality, it exhibits various electrical and charge responses to thermal stimuli. This simple and efficient fabrication method can be used as a promising platform for fabricating a variety of functional devices.
NPG Asia Materials (2017) **9,** e445; doi:10.1038/am.2017.168; published online 27 October 2017

INTRODUCTION

Plants have specialized functions to ensure their survival and reproduction in a great diversity of habitats. Some plants contain soft materials that confer combinational functions of deformability and electrochemical properties. For instance, stomata in a leaf have a hydraulic gating function by swelling/deswelling the guard cells in response to ion transport through charged cell membranes.[1,2] *Mimosa pudica* and *Venus flytrap* rapidly close their leaves in response to electrical and mechanical stimuli.[3,4] In addition, cellular membranes in plants have various functional features. As a halophyte, mangrove has a charged filtration function, filtering sodium ions in saline water through its roots with a highly negative charged porous membrane.[5] Protein channels in the cellular membranes of vascular plants have a stimulus-responsive filtering function that allows specific biomolecules to pass through the membrane.[6] To mimic these special functionalities, stimulus-responsive hydrogels have been widely employed owing to their unique porous structures and swelling/deswelling ability in response to various environmental stimuli.[7,8] However, most conventional bio-inspired systems mimic only simple structural motions by using nonconductive hydrogels.[9–12]

To enhance the electrical functionality of stimulus-responsive hydrogels, conducting materials such as fillers, graphene and polymers can be incorporated into hydrogels.[13–18] For instance, conductive polymer (CP) hydrogels contain conjugated conductive backbones to promote charge transport and exhibit semiconducting electrical properties.[19] Thus, CP hydrogels have the distinctive properties of a hydrogel and the electrical properties of CPs. Their potential has been demonstrated in a broad range of applications, such as in energy conversion and storage devices, supercapacitors, sensors, bioelectronics and medical electrodes.[20–23] The incorporation of CPs, such as polypyrrole, polyaniline and polythiophene, with a variety of polymers, metals, membranes and bioactive molecules, has been extensively studied due to their ease of synthesis, processability, and excellent environmental stability.[24–26] However, CPs are difficult to further modify after synthesis using post-processing methods, because they are normally non-thermoplastic, mechanically rigid and insoluble.[22,27] To improve the performance of CPs, a diverse set of architectures have been adopted and applied, because well-defined architectures are highly important in materials science, nanotechnology and bioengineering.[19,28–30] However, direct and precise patterning of various architectures is still a major challenge because the conventional technologies that are used to produce designed polymers have poor reproducibility and involve multiple fabrication steps, which makes the process expensive, time-consuming and difficult to scale-up.[30]

In this study, inspired by the functional features of plants, such as the bending of the pulvinus in *M. pudica*, the gating of stomata in leaf, and the selective filtering of the cellular membrane, a multifunctional hybrid membrane (HM) with thermo-responsive and conductive

Department of Mechanical Engineering, Pohang University of Science and Technology, Pohang, Republic of Korea
Correspondence: Professor SJ Lee, Department of Mechanical Engineering, Pohang University of Science and Technology, Pohang, Room 210, Mechanical Engineering Experimental Building, 77 Cheongam-Ro, Nam-Gu, Pohang-si, 37673, Gyeongbuk, Republic of Korea.
E-mail: sjlee@postech.ac.kr
Received 27 March 2017; revised 6 June 2017; accepted 28 June 2017

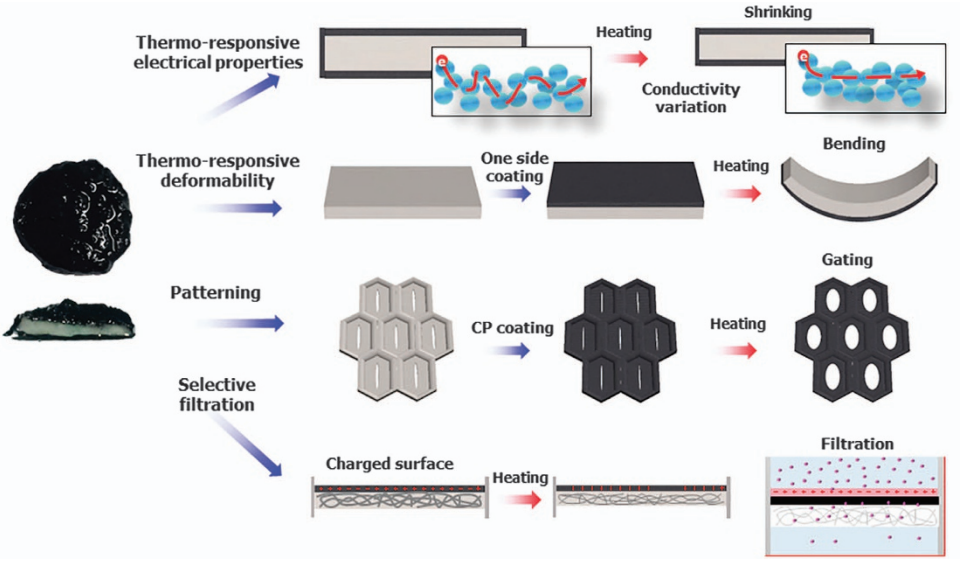

Figure 1 Unique combined features of PNIPAm and PPy provide innovative multiple functions. Thermo-responsive volumetric change induces deformable bending or variation in electrical conductivity. Membranes of various shapes can be fabricated by utilizing photopolymerization patterning. Variation in membrane surface charge can be used for selective filtration of charged molecules.

properties was adaptively synthesized with poly(*N*-isopropylacrylamide) (PNIPAm) and poly(pyrrole) (PPy), to enhance the functionalities of conventional CP hydrogels. PNIPAm and PPy are a representative thermo-responsive hydrogel and a CP, respectively. A thermo-responsive PNIPAm membrane (PM), which is used as a building block for the proposed structure, is fabricated by photopolymerization patterning tailored for its intended use, and the CP PPy is *in situ* polymerized on the PM. The morphological and electrical properties were measured to characterize the fabricated HM. The adaptive combination of the unique properties of PNIPAm and PPy confers various innovative functions of thermo-deformability, thermo-responsive electrical properties and thermo-responsive surface charge (Figure 1). By overcoming the limitations of conventional technologies used to produce patterned CPs, the proposed method is inexpensive and simple for the fabrication of large-scale functional membranes with various structures. Moreover, the thermo-responsive volumetric change of PNIPAm imparts reversible flexibility to non-thermoplastic and rigid PPy. This technique may open a new world of multifunctional smart materials with novel properties for the design of electrical and electrochemical devices.

MATERIALS AND METHODS

Fabrication of the HM

Photocrosslinkable PM was synthesized by free radical polymerization. A pre-gel solution was prepared by dissolving 100 mg of *N*-isopropylacrylamide monomer (Sigma-Aldrich) in 0.7 ml of deionized water. Subsequently, *N*,*N*′-methylenebisacrylamide (Sigma-Aldrich; 1 mg for the moderately crosslinked (MC) membrane, 3 mg for the highly crosslinked (HC) membrane) and 1 mg of 2-hydroxy-1-[4-(hydroxyethoxy)phenyl]-2-methyl-1-propanone (Irgacure 2959; Sigma-Aldrich) were added to the monomer solution as a crosslinker and photoinitiator, respectively. The pre-gel solution was covered with a transparent photomask, onto which specified patterns were printed and irradiated with UV light (VIRVER Lourmat-4.L, France; $\lambda = 365$ nm, 4 W) for 4 min. The fabricated membrane was carefully peeled from the photomask and stored in distilled water to fully hydrate the membrane and dissolve excess reactants. After cleaning, the PM was heated at 50 °C to completely deswell it and was then immersed in a pyrrole monomer solution (Supplementary Figure S5). The shrunken PM was fully swelled again as the PM favorably absorbed the pyrrole solution. Ammonium persulfate (283 mg) and the phytic acid solution (0.921 ml) were dropped onto the PM, and the CP was formed through *in situ* polymerization. The obtained HM was immersed in deionized water to remove unreacted residue.

Characterizations of the HM

The surface morphologies of the fabricated membranes were observed using a digital camera (NIKON D700, Tokyo, Japan) attached to a stereoscope (Stemi 2000c, Zeiss, Germany). The detailed morphological structures of the freeze-dried membranes were examined using a field-emission scanning electron microscope (JEOL JSM-7401F, JEOL Ltd., Tokyo, Japan).

The swelling ratio based on weight is defined as follows: $(m_f - m_i)/m_i$, where m_f and m_i are the final and initial masses of the membrane, respectively. The strain is defined as $(L_f - L_i)/L_i$, where L_f and L_i are the final and initial lengths of the membrane, respectively. The electrical resistance of the flat membrane was carefully measured using a four-point probe method (Keithley 236 current source and Keithley 617 electrometer, Keithley instruments, Inc., Cleveland, OH, USA), and that of the patterned membrane was measured using a two-point probe method (Fluke 189, Everett, WA, USA). The prepared membranes are placed on a completely non-conducting surface. Two metal measurement probes are placed at the ends of the membrane. Surface conductivity is calculated using the equation $\sigma = \frac{1}{\rho} = \frac{l}{R \cdot A}$, where σ is the electrical conductivity, ρ is the electrical resistivity, R is the electrical resistance, l is the distance between the two measurement points and A is the contact surface area where the measurement probes are touched. The thermal response of the prepared membranes was realized by heating the membrane above the low critical solution temperature (LCST) of the PNIPAm (33 °C). After the volumetric changes were completed, the membranes were cooled to room temperature again and the conductivities were measured. Young's moduli of the membranes before and after heating were evaluated using a Universal Testing Machine (Instron 3344, Instron Ltd., Norwood, MA, USA).

The filtration performance of the prepared membranes was estimated by measuring the water flux through the membranes. The solution flux (J) was evaluated from the temporal mass variation of filtered water as measured by a microbalance (Analytical Plus, AP250D, Ohaus, Florham Park, NJ, USA). The relative flux (J/J_0) is calculated by dividing the water flux by the initial water flux. The test membranes were inserted between silicone gaskets used for sealing and tightened with acrylic holders (Figure 6a). Deionized water or 0.15 g l^{-1} bovine serum albumin (BSA) (Sigma-Aldrich) solution was supplied to the reservoir, to apply a hydrostatic pressure of $P = \rho gh/A$ to the membrane. Here, ρ is the fluid density, g is the gravitational acceleration, h is the height of the solution from the membrane and A is the test area of the membrane.

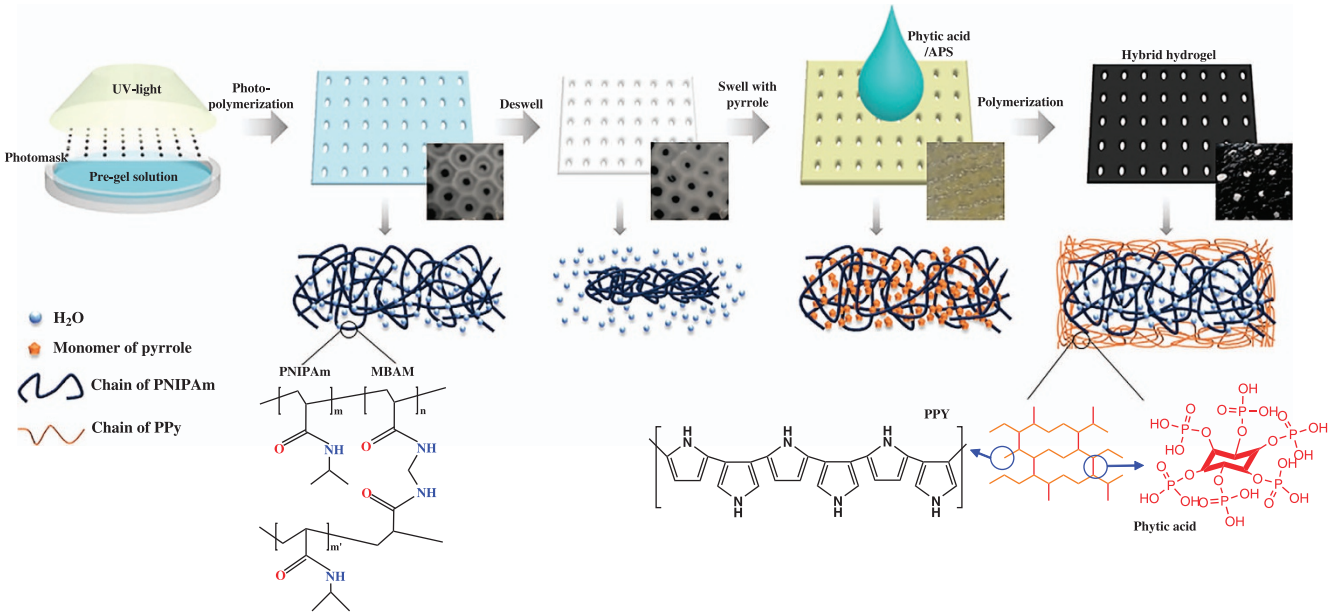

Figure 2 Schematic illustration of synthesis process of the HM. *N*-isopropylacrylamide monomer (NIPAm) monomer is crosslinked by *N,N'*-methylenebisacrylamide (MBAM) through photopolymerization with an arbitrarily patterned photomask, and the PM is then fabricated. The PM membrane is dehydrated by heating to a temperature above the LCST and reswollen in pyrrole monomer solution. The solution of phytic acid and ammonium persulfate (APS) is then dropped on the PM to allow *in situ* polymerization of conductive PPy. Optical images show fabricated membranes at each synthesis stage.

The filtered water was then drained through the outlet. The hydraulic resistance of the HM is higher than that of the PM, because the polymer network of the HM is thicker and denser. Therefore, a higher hydrostatic pressure is required to make the solution penetrate the HM membrane. Thus, the solution is supplied to the reservoir up to a height of $h = 3$ cm for the PM cases and $h = 8.5$ cm for the HM cases. When the effect of temperature on protein filtration was investigated, the temperature of the BSA solution was increased from room temperature to 45 ~ 48 °C, which is higher than the LCST of the PNIPAm but lower than the transition temperature of the BSA molecules.[31,32]

RESULTS AND DISCUSSION

Fabrication of the HM

The synthesis of the HM is illustrated in Figure 2. A UV-curable PM is used as the building block for the structure and fabricated by photopolymerization. A photocrosslinkable pre-gel solution is then illuminated with UV light using a patterned photomask. At a temperature above the LCST of PNIPAm of 32 °C, the PNIPAm network is completely shrunk by extruding water molecules. Dropping a monomer solution of pyrrole onto the deswelled PM enables it to reswell. Then, a solution of phytic acid and ammonium persulfate, which are a crosslinker and oxidant initiator, respectively, is dropped on the reswollen PM for *in situ* polymerization of CP chains. Phytic acid reacts with the PPy chains by protonating nitrogen groups, resulting in the formation of a polymer network.[23] As the PM can be arbitrarily patterned through photopolymerization, the final HM could be fabricated into various shapes to meet the needs of the intended applications. In addition, as PNIPAm exhibits thermo-responsive volumetric variation, the volume of the fabricated HM also varies with thermal stimuli.

A cross-sectional image of the fabricated hydrogel shows that the white color of PM is sandwiched between the blue-black PPy layers (Figure 1 and Supplementary Figure S1). Immediately after dropping the crosslinker on the PM, which is swollen by pyrrole, crosslinking occurs and a thin film of PPy whose thickness averages 76.08 ± 6.64 μm is rapidly formed on the surface of the PM. Therefore, the crosslinker solution cannot permeate deeply into the network of PNIPAm and only the surface of the PM is covered with PPy. If the undeformable PPy deeply penetrated into the PNIPAm, it may largely lose its thermo-responsive deformability.

Thermo-responsive morphological and electrical properties of the HM

More detailed investigations of the morphological and microstructure of the swollen and shrunken MC-HMs were performed using scanning electron microscopy (Figures 3a–f). When the HM is swollen, the interface between PNIPAm and PPy is slightly entangled by polymer branches, but the PPy does not penetrate deeply into the PNIPAm as expected (Figure 3a). The MC PNIPAm forms a continuous interconnected network with branched microfibers at a 10 μm pore scale (Figure 3b). Most PPy layers have porous globular structures and the average diameter of the globular particles is ~ 170 nm (Figure 3c). The globular particles are aggregated into chain-shaped or large-scale globular forms. Typical scanning electron microscopy images of the shrunken MC-HM shows that the interface between the PNIPAm and PPy is more tightly entangled by an interconnected polymer network, compared with that of swollen HM (Figure 3d). Individual microfibers of PNIPAm and the globular structures of the PPy are also more densely packed than those of swollen HM (Figures 3e and f).

Thermo-responsive volumetric changes can give rise to altered membrane electrical properties. To determine whether the fabricated HM can be used as a suitable material for deformable electrodes, variations in the resistance of the shrinking HM upon heating were measured using a four-point probe method. For this experiment, MC-HM was used as a test sample, because it has a high volumetric variation, which maximizes the effect of the thermo-responsive electrical properties. The electrical resistivity of the MC-HM is 90.63 Ωm and the corresponding conductivity is 0.02 ± 0.01 S m^{-1} at room temperature (Figure 3g). When the membrane is in the shrunken state due to heating, its electrical resistivity decreased to 15.99 Ωm

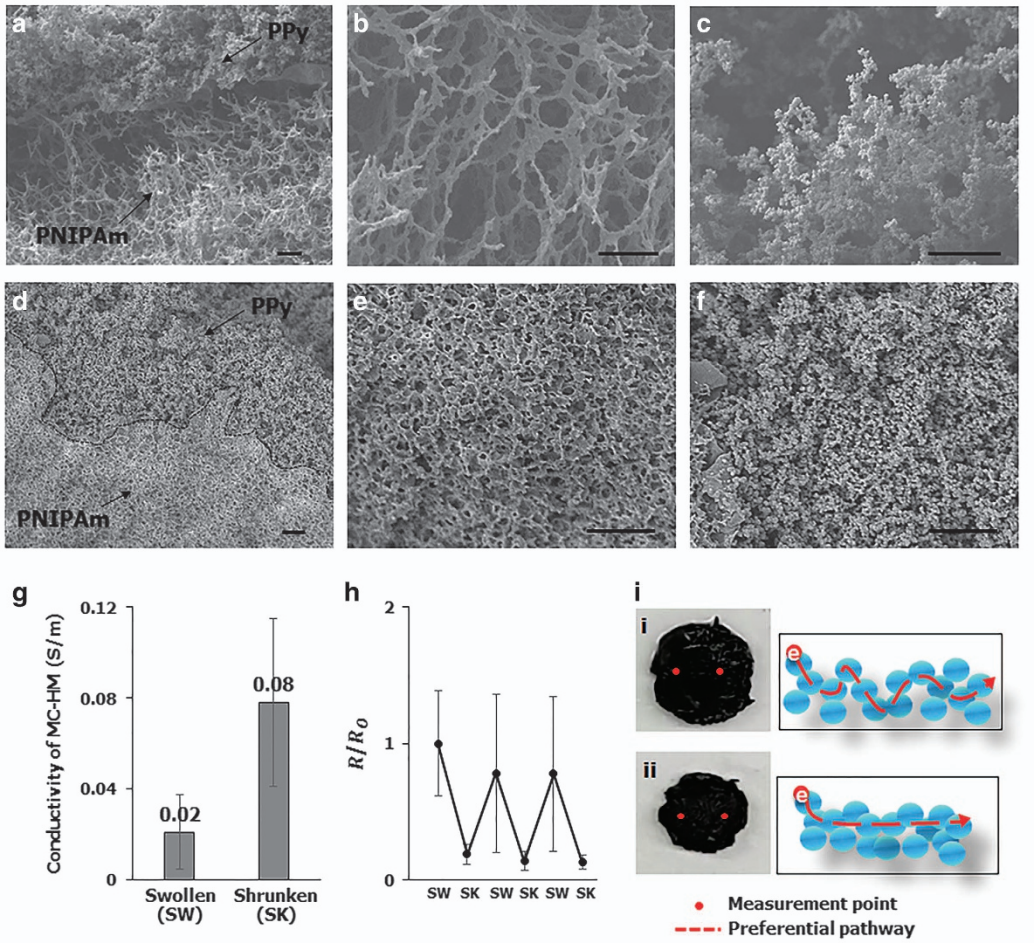

Figure 3 Thermo-responsive morphological structures and electrical properties of the fabricated MC-HM. Scanning electron microscopy (SEM) images of the swollen MC-HM at the (**a**) interface of PNIPAm and PPy, (**b**) PNIPAm and (**c**) PPy. SEM images of the shrunken MC-HM at the (**d**) interface of PNIPAm and PPy, (**e**) PNIPAm and (**f**) PPy. (**g**) Comparison of electrical conductivity of the membrane at swollen and shrunken states. (**h**) Variation of the normalized membrane resistance according to the cyclic repetition of shrunken and swollen states. (**i**) Conductivity increased due to the shortened preferential pathways because randomly polymerized PPy globular structures are more densely packed by volumetric shrinkage. (i) The MC-HM in the swollen state. (ii) The MC-HM after shrinking. The two red dots indicate the measurement points where two metal measurement probes are placed to measure electrical resistance. The blue circles represent the globular structures of PPy and red dotted lines are the imaginary preferential pathways of electrons. Scale bar: 10 μm.

and the corresponding conductivity increased to 0.08 ± 0.03 S m^{-1}. The geometric specifications of a polymer, such as polymer chain length, interconnection or conjugation region length, are important factors determining electrical resistance. The internal microscopic structure of the MC-HM changed as the temperature approached the structural transition. As the MC-HM reversibly shrinks/swells in response to heating/cooling, the electrical resistance of the MC-HM also reversibly responds to the temperature variation. The normalized resistance (R/R_0) of the MC-HM decreased and increased several times, as it repeatedly shrank and swelled (Figure 3h). The conductivity might increase due to shortened preferential pathways, because the randomly polymerized PPy globular structures are packed closer together due to volumetric shrinking (Figures 3f and i (i, ii)).[16,33] Meanwhile, the measured values exhibited hysteresis with a large deviation. The geometric reversibility and conductivity recovery of a material are determined by the initial state of the polymer network. As the PNIPAm and PPy matrixes are very randomly fabricated, the hysteresis variation is caused by random rearrangement of the globular structures of the polymers, which prevents a return of the gel to its initial structure.

Thermo-responsive deformability of the HM

As water molecules are extruded from the PNIPAm network when the temperature increases above the LCST, the membrane exhibits volumetric shrinkage. As the degree of volume transition in the PNIPAm is tuned by the degree of crosslinking, MC and HC membranes are fabricated (Supplementary Figure S2). The Young's moduli of the MC-HM and HC-HM hydrogels in the swollen state are 5.91 and 10.03 kPa, respectively (Supplementary Figure S3). As the Young's modulus of the MC membrane is smaller than that of HC, MC has higher deformability than the HC membrane. After heating the membrane, the Young's moduli of MC-HM and HC-HM increased to 6.461 and 12.88 kPa, respectively.

To examine the thermal response of the fabricated membranes, the swelling ratio of each membrane, which indicates the degree of water extrusion from a polymer, was measured by heating the membranes above the LCST of the PNIPAm. When the PNIPAm is MC, the weight-swelling ratios of the fabricated PM and HM are 0.56 and 0.45, respectively (Figure 4a). When the PNIPAm is HC, the weight-swelling ratios of the PM and HM are 0.35 and 0.24, respectively (Figure 4b). Although the swelling ratios of the HMs

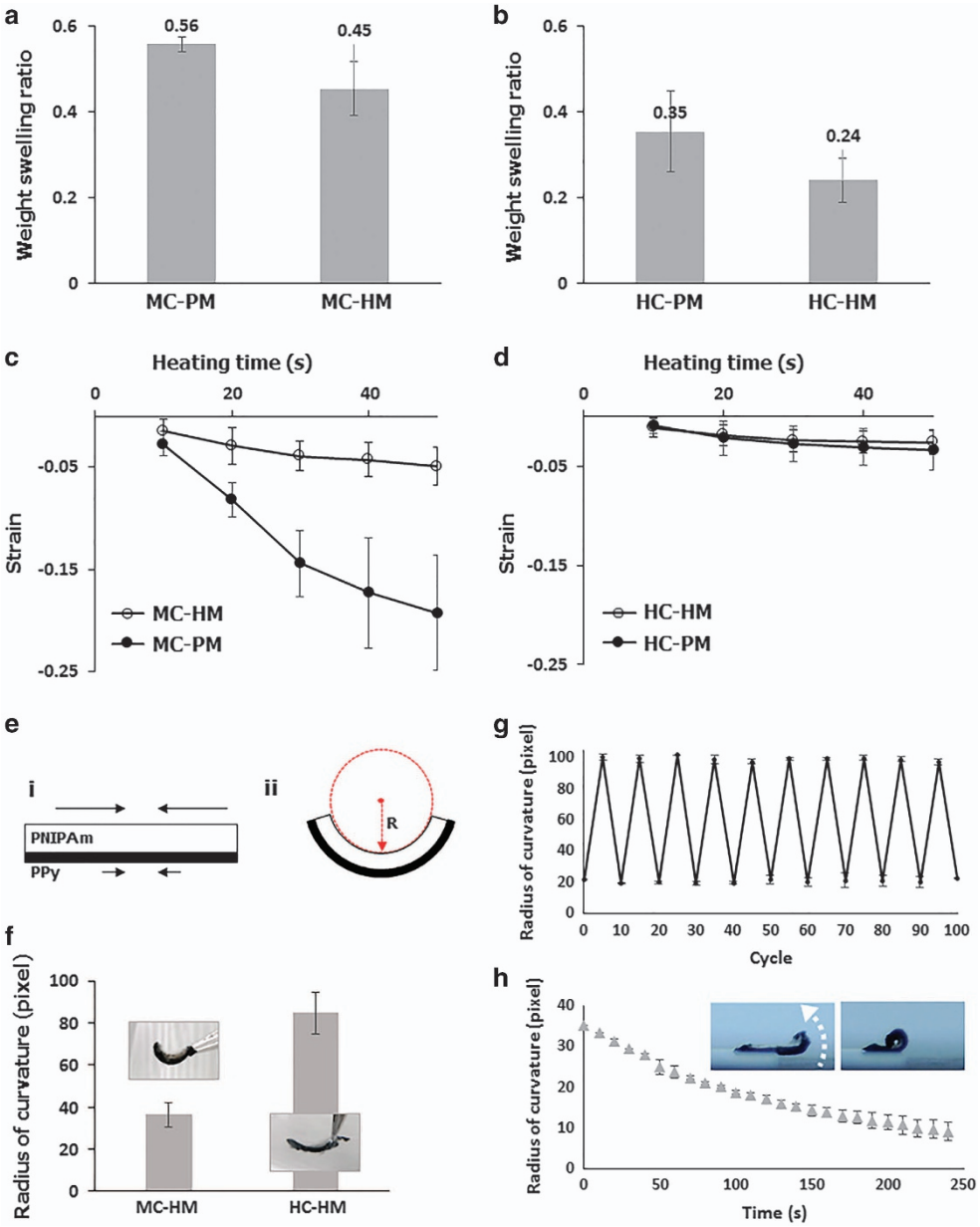

Figure 4 Thermo-responsive deformability of the fabricated membrane. Weight swelling ratios of (**a**) the MC membranes and (**b**) the HC membranes. Temporal variations of strain values of (**c**) the MC membranes and (**d**) the HC membranes. (**e**) Schematic illustration of the bending motion of the bilayer HM actuator. (**f**) Comparison of radii of curvature of the MC-actuator and HC-actuator after bending. (**g**) Variation in the radius of curvature of the cyclic bending of the MC-actuator. (**h**) Temporal variation in the radius of curvature of the HC-actuator during lifting motion.

decreased after coating with PPy, they maintained the thermo-responsive volumetric transition feature of the PNIPAm. The comparative results of the fabricated MC and HC membranes show that the swelling ratios decrease as the crosslinker concentration increases.

To investigate the thermo-deformability of the fabricated membranes, strain as a function of time during heating was measured (Figures 4c and d). As the membranes were heated, all strain values decreased, indicating that the membranes shrank. During the initial 50 s of heating, the MC-PM shrinks almost 19.2% on average from its original length, whereas MC-HM shrinks ~4.9% from its original length (Figure 4c). The lower deformability of the HM is attributed to the non-deformable PPy, which constrains the shrinkage of the PM. By contrast, the HC-PM shrinks 3.4% on average and the HC-HM shrinks 2.6% from their original lengths in the initial 50 s of heating (Figure 4d). The difference in the length shrinkage ratios of the PM and HM for HC membranes is smaller than the MC membrane.

The difference in the deformabilities of the PM and HM induces the bending or lifting of the membranes. To demonstrate such motion in the membranes, a bilayer actuator was fabricated, in which one side is the PM and the other side is the HM (Figure 4e). The bilayer actuators were then dipped in hot water (65 °C). As the PM shrinks more than the HM, the heated membrane bends toward the PM layer. The bending motion of the actuator occurs within 2 s after the device is heated or cooled, demonstrating the high thermo-responsive

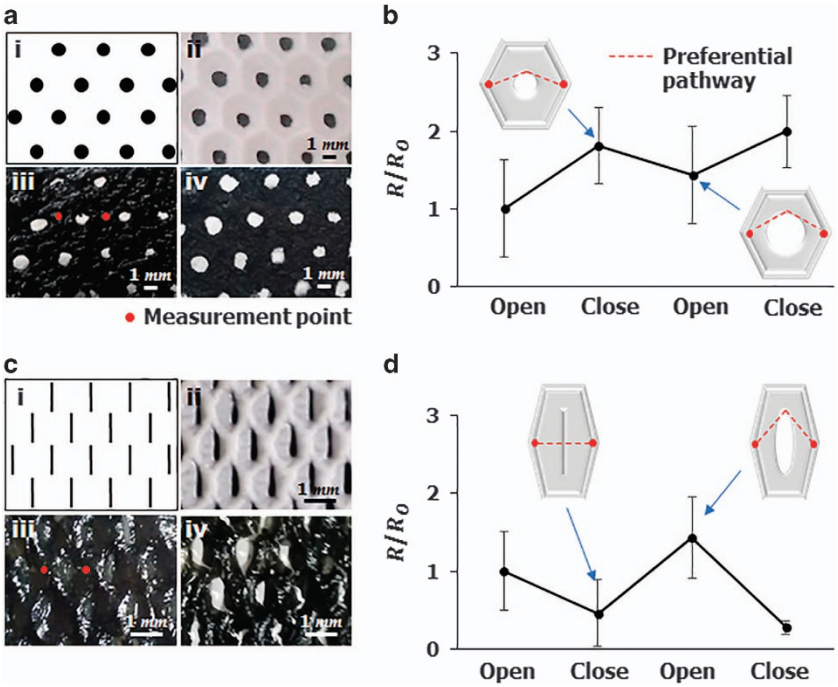

Figure 5 Two typical patterns of the HM. (**a**) Honeycomb-shaped HM. (i) Honeycomb-shaped PM fabricated using the dotted photomask. (ii) Holes are formed just under the dotted patterns, and relatively thicker frames are formed between holes. (iii) As the PPy is *in situ* coated on the PM surface, a HM with holes formed. The two red dots indicate the measurement points where two metal probes are placed to measure resistance. (iv) The holes widen when heating to a temperature higher than the LCST. (**b**) Normalized resistance varies as holes in the honeycomb-shaped membrane open/close. The red dotted lines are imaginary preferential pathways of electrons. (**c**) (i ~ iv) Fabrication of hexagonal HM using a photomask with a pattern of vertical slits. (**d**) Normalized resistance varies as holes in the hexagon-shaped membrane open/close.

sensitivity of the actuator. As the deformability between the MC-PM and MC-HM is greater than between the HC-PM and HC-HM, the final radius of curvature of the MC actuator is smaller than that of the HC actuator (Figure 4f). This result supports that the bending motion of the HM that can be easily controlled by adjusting the degree of PM crosslinking.

The cycling variation of bending motion was further tested to demonstrate the dynamic stability of the actuator. Figure 4g shows the periodic variation in the radius of curvature of the MC-actuator during 100 cycles of heating and cooling. The radius of curvature maintains ~98 pixels under the heating condition and ~22 pixels under the cooling condition, even after 100 cycles of heating and cooling. This result implies that the HM does not lose its deformability, even after many cyclic temperature variations. When the membrane was continuously heated until most water molecules in the hydrogel were removed, the bilayer actuator lifted and rolled toward the PM layer, overcoming gravitational force (Figure 4h, Supplementary Figure S4 and Supplementary Movie S1). When the deformed actuator was cooled by dipping it into room temperature water, it reversibly absorbed water and again stretched to its original shape. This controllability of deformation is useful for making mechanical actuators, sensors, and soft robots.

Patterning of the HM

The photopolymerized PMs can be arbitrarily patterned using variously patterned photomasks. As a typical example, a honeycomb-shaped HM was fabricated using a dotted photomask (Figure 5a (i, ii) and Supplementary Figure S5). Immediately under the dotted pattern of the photomask where UV light is blocked, circular pores formed and relatively thicker frames formed between the pores (Figure 5a (ii)).[34] Through the *in situ* coating of the PPy on the patterned PMs, a honeycomb-shaped HM was realized (Figure 5a (iii)). The pores of the membrane have a gating function as the membrane is heated and cooled (Figure 5a (iv)). During heating of the membrane, stress-induced shrinkage considerably increased the size of circular pores. In accordance with the opening of pores, the normalized resistance slightly decreased (Figure 5b). As the membrane cooled, pore size decreased and normalized resistance slightly increased. This result may be attributed to variation in the preferential pathway of electrons, which is lengthened/shortened by heating/cooling (red dotted lines). The normalized resistance varies depending on the morphologies and gating configuration of the membrane. When a photomask with a pattern of vertical slits was used, a hexagonal HM was fabricated (Figure 5c (i, ii)). The membrane has vertical slit-shaped pores, which are initially almost closed (Figure 5c (iii)). As the membrane was heated, the slits opened and expanded into an almost elliptical configuration (Figure 5c (iv)). The resistance variation in this case shows the opposite tendency to the honeycomb HM (Figure 5d). When the slits are closed, electrons directly pass through the connections across the slits and the preferential pathway is greatly shortened, decreasing the normalized resistance (red dotted line). When the slits open, the preferential pathway is elongated and the normalized resistance increases. When resistance was measured over the wider region covering several pores or slits, the variation tendency of the resistance according to gating of pores or slits is the same. As the membrane exhibits a variety of movements depending on the design of membrane structure, the conductivity also varies widely according to the movements. Therefore, the membrane can be used in various practical applications.

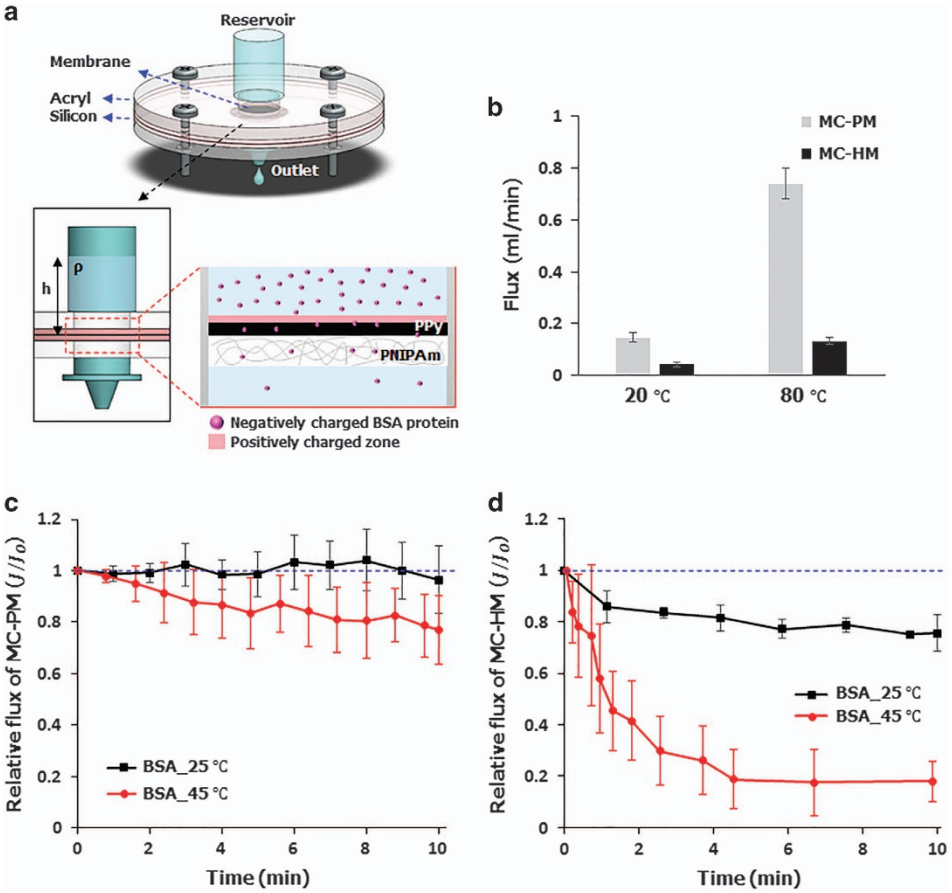

Figure 6 Thermo-responsive filtration of charged proteins. The MC membrane is applied as a filter membrane for separation of BSA from water. (**b**) Water flux through membranes increases in accordance with increased temperature. The water permeability of the MC-PM is higher than the MC-HM. (**c**) Temporal variations of relative flux of BSA solution through the MC-PM. (**d**) Temporal variations of the relative flux of BSA solution through the MC-HM.

Thermo-responsive filtration of charged proteins

As an important practical application, the HM was used as the thermo-responsive filter membrane for the separation of proteins from water. PNIPAm-grafted filter membranes and PPy filter membranes have been used to separate nano/micro molecules.[35–38] The surface zeta potential and wettability of membranes are important material properties to determine hydraulic resistance, which is a measure of the filtration performance of the membrane. As the surface zeta potential varies with temperature, the filtration effect caused by electrostatic interaction also varies with temperature.[39,40] To investigate the charge effect of the MC membranes in response to thermal stimuli, the water flux through the membrane under hydrostatic pressure was measured as a function of temperature (Figure 6a). The high volumetric variations of flow through the MC membranes demonstrated the thermo-responsive charge effect.

When deionized water was applied, the water flux through the membranes increased with increasing temperature. This result implies that the water permeability of the membrane increases with increasing pore size (Figure 6b). The wettability of the membranes also changed with temperature, which is due to the transition of the thermo-responsive wettability of PNIPAm from hydrophilic to hydrophobic.[41] The water flux through the MC-HM was smaller than that of the MC-PM. This effect results from the increase of hydraulic resistance due to deposition of the more densely crosslinked PPy network.

When a solution of negatively charged BSA was used, both MC-PM and MC-HM exhibited the ability to exclude the protein. The relative fluxes (J/J_0) of the filtered solution through the membranes decreased with time in most cases, where J is the flux and J_0 is the initial flux of the solution. However, the tendency to decrease varied depending on the membranes (Figures 6c and d). When the MC-PM was used and 25 °C BSA solution was applied, the flux was almost constant for 10 min of filtration (Figure 6c). When the solution temperature increased to ~45 °C, the flux gradually decreased and reached 77% of the initial flux after 10 min. When 0.15 g l^{-1} acidic BSA solution at pH 5.5 was applied, the surface zeta potential of PNIPAm was negative; at approximately −3 mV at 25 °C and decreasing to approximately −10 mV at 45 °C.[40] The negative zeta potential on the membrane surface acts as an electrostatic barrier against the negatively charged BSA molecules.[37] Proteins are pushed back from the membrane surface by electrostatic force, which acts as a hydraulic resistance barrier. Therefore, the relative flux is reduced. As the BSA solution is maintained at 45–48 °C during the experiment, the size effect of BSA aggregates is negligible. As the transformation temperature of BSA is 70 °C, heat-induced irreversible intermolecular transformation does not occur in the experiment.[31,32]

The filtration effect of the MC membranes is more definite. After filtering for 10 min at room temperature, the relative flux through the membrane decreased by 25%, compared with the initial flux (Figure 6d). This decrease is attributed to the electrical charge of the MC membranes. The PPy surface has a positive zeta potential in acidic solution when 0.15 g l^{-1} acidic BSA solution at pH 5.5 is applied.[42] Owing to the electrical attraction between the PPy surface and BSA

molecules induced by their opposite polarity, some proteins adhered to the charged PPy surface.[37,38,43] The adsorbed proteins on the membrane surface increase hydraulic resistance. Hence, the flux of the filtered solution through the membrane is decreased. As the temperature increases to 45 °C, the relative flux of the filtered solution rapidly decreased to only 18% of the initial flux after 10 min of filtering (Figure 6d). As the surface zeta potential normally increases with increasing temperature, the BSA molecules are more favorably adsorbed on the PPy surface, which intensifies the degradation of the membrane filtration performance.[39]

CONCLUSION

Inspired by the stimuli-responsive functional systems in plants, a new multifunctional HM composed of a thermo-responsive hydrogel and a CP was fabricated in an easy and simple manner. Thermo-responsive PM, which is used as a building block, is patterned by photopolymerization in accordance with the intended use, and a CP PPy is coated onto the PM. The fabricated HM exhibits multiple thermo-responsive functions, including deformability, variation in electrical properties and changes in surface charge. When the PNIPAm and PPy bilayer actuator is heated above the LCST, it bends or rolls as the pulvinus of Mimosa does. When pores are formed in the membrane by utilizing photopolymerization patterning, they possess a gating function with varying electrical potential in response to temperature stimuli, as stomata do. These special properties demonstrate strong potential in the fabrication of bioactuators or soft robots. As volumetric changes caused by thermal stimuli can induce variation in electrical resistance, this functional feature can be utilized as a biosensor. As the surface zeta potential of the HM is changed by thermal stimuli, the electrostatic interaction of charged molecules with the membrane can also be effectively modulated. This functional membrane would be a good candidate for selective filtering of solutions, as the porous membrane of plant roots does. With these multiple functions and a simple yet efficient fabrication process, the present HM has great potential to open a new era of stimulus-responsive hydrogels.

CONFLICT OF INTEREST

The authors declare no conflict of interest.

ACKNOWLEDGEMENTS

We thank the National Institute for Nanomaterials Technology (Pohang, Korea) and Gyeongyun Go in the Department of Life Science, POSTECH, for help in performing the experiments for scanning electron microscopy and freeze-drying the samples. We also appreciate Hyunah Kwon in the Department of Materials Science and Engineering, POSTECH, who helped perform the four-point probe method measurements. This work was supported by the National Research Foundation of Korea (NRF) grant funded by the Korean government (MSIP) (number 2017R1A2B3005415).

Author contributions: H.K., K.K. and S.J.L. proposed the study. H.K. and K.K. performed the experiment, processed images and analyzed experimental data. All authors discussed the results and participated in completing the manuscript.

PUBLISHER'S NOTE

1 Willmer, C. & Fricker, M. *Stomata*, 2nd edn (Chapman & Hall: London, 1996).
2 Keller, B. U., Hedrich, R. & Raschke, K. Voltage-dependent anion channels in the plasma membrane of guard cells. *Nature* **341**, 450–453 (1989).
3 Song, K., Yeom, E. & Lee, S. J. Real-time imaging of pulvinus bending in *Mimosa pudica*. *Sci. Rep.* **4**, 6466 (2014).
4 Volkov, A. G., Adesina, T. & Jovanov, E. Closing of *Venus flytrap* by electrical stimulation of motor cells. *Plant Signal. Behav.* **2**, 139–145 (2007).
5 Kim, K., Kim, H., Lim, J. H. & Lee, S. J. Development of a desalination membrane bioinspired by mangrove roots for spontaneous filtration of sodium ions. *ACS Nano* **10**, 11428–11433 (2016).
6 Maurel, C., Verdoucq, L., Luu, D. T. & Santoni, V. Plant aquaporins: membrane channels with multiple integrated functions. *Annu. Rev. Plant Biol.* **59**, 595–624 (2008).
7 Stuart, M. A. C., Huck, W. T., Genzer, J., Müller, M., Ober, C., Stamm, M., Sukhorukov, G. B., Szleifer, I., Tsukruk, V. V. & Urban, M. Emerging applications of stimuli-responsive polymer materials. *Nat. Mater.* **9**, 101–113 (2010).
8 de las Heras Alarcón, C., Pennadam, S. & Alexander, C. *Chem. Soc. Rev.* **34**, 276–285 (2005).
9 Ionov, L Biomimetic hydrogel-based actuating systems. *Adv. Funct. Mater.* **23**, 4555–4570 (2013).
10 Guo, Q., Dai, E., Han, X., Xie, S., Chao, E. & Chen, Z. Fast nastic motion of plants and bioinspired structures. *J. R. Soc. Interface* **12**, 0598 (2015) 20150598.
11 Li, S. & Wang, K. Plant-inspired adaptive structures and materials for morphing and actuation: a review. *Bioinspir. Biomim.* **12**, 011001 (2016).
12 Ma, C., Shi, Y., Pena, D. A., Peng, L. & Yu, G. Thermally responsive hydrogel blends: a general drug carrier model for controlled drug release. *Angew. Chem. Int. Ed. Engl.* **127**, 7484–7488 (2015).
13 Tai, Y., Mulle, M., Ventura, I. A. & Lubineau, G. A highly sensitive, low-cost, wearable pressure sensor based on conductive hydrogel spheres. *Nanoscale* **7**, 14766–14773 (2015).
14 Shi, Y., Pan, L., Liu, B., Wang, Y., Cui, Y., Bao, Z. & Yu, G. 'Nanostructured conductive polypyrrole hydrogels as high-performance, flexible supercapacitor electrodes.' *J. Mater. Chem. A* **2**, 6086–6091 (2014).
15 Annabi, N., Tamayol, A., Uquillas, J. A., Akbari, M., Bertassoni, L. E., Cha, C., Camci-Unal, G., Dokmeci, M. R., Peppas, N. A. & Khademhosseini, A. 25th Anniversary article: rational design and applications of hydrogels in regenerative medicine. *Adv. Mater.* **26**, 85–124 (2014).
16 Imran, S. M., Shao, G. N., Haider, M. S., Abbas, N., Hussain, M. & Kim, H. T. Electroconductive performance of polypyrrole/graphene nanocomposites synthesized through in situ emulsion polymerization. *J. Appl. Polym. Sci.* **132**, 41800 (2015).
17 Shi, Y., Zhang, J., Pan, L., Shi, Y. & Yu, G. Energy gels: a bio-inspired material platform for advanced energy applications. *Nano Today* **11**, 738–762 (2016).
18 Shi, Y., Ha, H., Al-Sudani, A., Ellison, C. J. & Yu, G. Thermoplastic elastomer-enabled smart electrolyte for thermoresponsive self-protection of electrochemical energy storage devices. *Adv. Mater.* **28**, 7921–7928 (2016).
19 Pan, L., Yu, G., Zhai, D., Lee, H. R., Zhao, W., Liu, N., Wang, H., Tee, B. C.-K., Shi, Y. & Cui, Y. Hierarchical nanostructured conducting polymer hydrogel with high electrochemical activity. *Proc. Natl Acad. Sci. USA* **109**, 9287–9292 (2012).
20 Zhao, Y., Liu, B., Pan, L. & Yu, G. 3D nanostructured conductive polymer hydrogels for high-performance electrochemical devices. *Energy Environ. Sci.* **6**, 2856–2870 (2013).
21 Barthus, R. C., Lira, L. M. & Torresi, S. I. Conducting polymer-hydrogel blends for electrochemically controlled drug release devices. *J. Brazil. Chem. Soc.* **19**, 630–636 (2008).
22 Balint, R., Cassidy, N. J. & Cartmell, S. H. Conductive polymers: towards a smart biomaterial for tissue engineering. *Acta Biomaterial.* **10**, 2341–2353 (2014).
23 Shi, Y., Ma, C., Peng, L. & Yu, G. Conductive 'smart' hybrid hydrogels with PNIPAM and nanostructured conductive polymers. *Adv. Funct. Mater.* **25**, 1219–1225 (2015).
24 Hur, J., Im, K., Kim, S. W., Kim, J., Chung, D. –Y., Kim, T. –H., Jo, K. H., Hahn, J. H., Bao, Z. & Hwang, S. Polypyrrole/agarose-based electronically conductive and reversibly restorable hydrogel. *ACS Nano* **8**, 10066–10076 (2014).
25 Lu, Y., He, W., Cao, T., Guo, H., Zhang, Y., Li, Q., Shao, Z., Cui, Y. & Zhang, X. Elastic, conductive, polymeric hydrogels and sponges. *Sci. Rep.* **4**, 5792 (2014).
26 Liu, Y., Xu, K., Chang, Q., Darabi, M. A., Lin, B., Zhong, W. & Xing, M. Highly flexible and resilient elastin hybrid cryogels with shape memory, injectability, conductivity, and magnetic responsive properties. *Adv. Mater.* **28**, 7758–7767 (2016).
27 Kaur, G., Adhikari, R., Cass, P., Bown, M. & Gunatillake, P. Electrically conductive polymers and composites for biomedical applications. *RSC Adv.* **5**, 37553–37567 (2015).
28 Liu, S., Gordiichuk, P., Wu, Z. -S., Liu, Z., Wei, W., Wagner, M., Mohamed-Noriega, N., Wu, D., Mai, Y. & Herrmann, A. Patterning two-dimensional free-standing surfaces with mesoporous conducting polymers. *Nat. Commun.* **6**, 8817 (2015).
29 Yang, X., Zhao, Y., Xie, J., Han, X., Wang, J., Zong, C., Ji, H., Zhao, J., Jiang, S. & Cao, Y. Bioinspired fabrication of free-standing conducting films with hierarchical surface wrinkling patterns. *ACS Nano* **10**, 3801–3808 (2016).
30 Garcia-Cruz, A., Lee, M., Zine, N., Sigaud, M., Bausells, J. & Errachid, A. Poly (pyrrole) microwires fabrication process on flexible thermoplastics polymers: application as a biosensing material. *Sens. Actuators B Chem.* **221**, 940–950 (2015).
31 Murayama, K. & Tomida, M. Heat-induced secondary structure and conformation change of bovine serum albumin investigated by Fourier transform infrared spectroscopy. *Biochemistry* **43**, 11526–11532 (2004).
32 Moriyama, Y., Watanabe, E., Kobayashi, K., Harano, H., Inui, E. & Takeda, K. Secondary structural change of bovine serum albumin in thermal denaturation up to 130 C and protective effect of sodium dodecyl sulfate on the change. *J. Phys. Chem. B* **112**, 16585–16589 (2008).

33 Košina, S., Balúch, S., Annus, J., Omastová, M. & Krištín, J. Study on the electrical conductivity and morphology of porous polypyrrole layers prepared electrochemically in the presence of pyridinium chlorochromate. *J. Mater. Sci.* **29**, 3403–3407 (1994).
34 Kim, H. & Lee, S. –J. Fabrication of triple-parted stomata-inspired membrane with stimulus-responsive functions. *Sci. Rep.* **6**, 21258 (2016).
35 Liao, Y., Farrell, T. P., Guillen, G. R., Li, M., Temple, J. A., Li, X. -G., Hoek, E. M. & Kaner, R. B. Highly dispersible polypyrrole nanospheres for advanced nanocomposite ultrafiltration membranes. *Mater. Horizons* **1**, 58–64 (2014).
36 Wang, R., Zhou, Y., Huang, Y. -q. & Ghosh, R. Poly (N-isopropylacrylamide)-grafted dual stimuli-responsive filter paper for protein separation. *Chin. J. Polym. Sci.* **33**, 1048–1057 (2015).
37 Madaeni, S. S. & Molaeipour, S. Investigation of filtration capability of conductive composite membrane in separation of protein from water. *Ionics* **16**, 75–80 (2010).
38 Liu, L., Liu, J., Bo, G., Yang, F., Crittenden, J. & Chen, Y. Conductive and hydrophilic polypyrrole modified membrane cathodes and fouling reduction in MBR. *J. Membr. Sci.* **429**, 252–258 (2013).
39 Rodríguez, K. & Araujo, M. Temperature and pressure effects on zeta potential values of reservoir minerals. *J. Colloid Interface Sci.* **300**, 788–794 (2006).
40 Synytska, A., Svetushkina, E., Puretskiy, N., Stoychev, G., Berger, S., Ionov, L., Bellmann, C., Eichhorn, K. -J. & Stamm, M. Biocompatible polymeric materials with switchable adhesion properties. *Soft Matter* **6**, 5907–5914 (2010).
41 Kim, H. & Lee, S. J. 'Stomata-inspired membrane produced through photopolymerization patterning.' *Adv. Funct. Mater.* **25**, 4496–4505 (2015).
42 Zhang, X. & Bai, R. Surface electric properties of polypyrrole in aqueous solutions. *Langmuir* **19**, 10703–10709 (2003).
43 Huang, J., Wang, Z., Zhang, J., Zhang, X., Ma, J. & Wu, Z. A novel composite conductive microfiltration membrane and its anti-fouling performance with an external electric field in membrane bioreactors. *Sci. Rep.* **5**, 9268 (2015).

Supplementary Information accompanies the paper on the NPG Asia Materials website (http://www.nature.com/am)